Eur Radiol (2011) 21:1962–1969
DOI 10.1007/s00330-011-2123-5

MAGNETIC RESONANCE

Three-dimensional magnetic resonance spectroscopic imaging in the substantia nigra of healthy controls and patients with Parkinson's disease

Adriane Gröger · Grzegorz Chadzynski · Jana Godau · Daniela Berg · Uwe Klose

Received: 8 December 2010 / Revised: 4 February 2011 / Accepted: 24 February 2011 / Published online: 12 April 2011

Abstract
Objectives To investigate the substantia nigra in patients with Parkinson's disease three-dimensional magnetic resonance spectroscopic imaging with high spatial resolution at 3 Tesla was performed. Regional variations of spectroscopic data between the rostral and caudal regions of the substantia nigra as well as the midbrain tegmentum areas were evaluated in healthy controls and patients with Parkinson's disease.
Methods Nine patients with Parkinson's disease and eight age- and gender-matched healthy controls were included in this study. Data were acquired by using three-dimensional magnetic resonance spectroscopic imaging measurements. The ratios between rostral and caudal voxels of the substantia nigra as well as the midbrain tegmentum areas were calculated for the main-metabolites N-acetyl aspartate, creatine, choline, and *myo*-inositol. Additionally, the metabolite/creatine ratios were calculated.
Results In all subjects spectra of acceptable quality could be obtained with a nominal voxel size of 0.252 ml. The calculated rostral-to-caudal ratios of the metabolites as well as of the metabolite/creatine ratios showed with exception of choline/creatine ratio significant differences between healthy controls and patients with Parkinson's disease.
Conclusions The findings from this study indicate that regional variations in N-acetyl aspartate/creatine ratios in the regions of the substantia nigra may differentiate patients with Parkinson's disease and healthy controls.

Keywords Magnetic resonance spectroscopic imaging · MRSI · Substantia nigra · Parkinson's disease

Introduction

Parkinson's disease (PD) is one of the most common neurodegenerative diseases. Clinical diagnosis is based on the UK PD Brain Bank criteria [1] in the presence of the common symptoms like bradykinesia, rigidity, resting tremor, postural instability, disease progression and response to levodopa administration. In early stages of the disease the criteria are often not met and a clinical diagnosis is often difficult [1–4]. The definite diagnosis can only be established by *post mortem* histological examination. So far, no imaging method has been included in the UK PD Brain Bank criteria as a diagnostic tool to monitor disease progression.

Parkinson's disease is characterised by progressive degeneration of the dopaminergic neurons in the substantia nigra (SN), but the reason for neuronal loss is not yet understood. To assess the degeneration of the SN in vivo a non-invasive method is needed. Such a method might serve as a diagnostic tool in early cases that are not yet clinically clear.

Proton magnetic resonance spectroscopy (MRS) provides biochemical information about the investigated

A. Gröger · J. Godau · D. Berg
Department of Neurodegeneration, Hertie Institute for Clinical Brain Research and German Center for Neurodegenerative Disease (DZNE), University of Tuebingen, Tuebingen, Germany

G. Chadzynski · U. Klose
Department of Diagnostic and Interventional Neuroradiology, University Hospital Tuebingen, Tuebingen, Germany

A. Gröger (✉)
Hoppe-Seyler-Str. 3,
72076 Tübingen, Germany
e-mail: adriane.groeger@med.uni-tuebingen.de

tissue and can be used as a tool for non-invasive evaluation of neurodegenerative diseases [5]. The main metabolites which can be detected by MRSI in the brain are N-acetyl aspartate (NAA), creatine and phosphocreatine (Cr), choline containing metabolites (Cho), and *myo*-inositol (Ins) [6]. NAA is produced predominantly in neurons and is accepted as a putative marker of viable neurons. Therefore, it is a possible indicator of neuron loss. However, the complex functionality of NAA in the biochemistry and neurobiology of the central nervous system is still unexplained [7]. Cr is a key energetic metabolite and, therefore, a possible indicator of defective energy metabolism. It was shown that Cr levels change slowly with age and in neuropathological conditions [8–10]. Changes in Cho can occur due to altered neuronal membrane synthesis and degeneration. Elevated Cho levels may reflect myelin breakdown or cellular proliferation [11]. Ins is a pentose sugar, which was found in glial cells and in lower concentrations in neurons [12]. It has been discussed as a detoxification agent, an osmoregulator and an intracellular messenger [12]. Changes in Ins have also been discussed in several processes observed in neurodegenerative disorders and could be a marker for inflammatory processes involving microglia activation [13, 14].

Magnetic resonance spectroscopy (MRS) has already been performed in PD patients by several groups. In accordance with the pathological features of PD, the SN is one of the most interesting anatomical regions in which to perform MRS. However, the SN is a very small and heterogeneous region inside the midbrain [15] with a high cellular iron content [16]. Local iron-induced magnetic field inhomogeneities [17] and field inhomogeneities caused by the magnetic susceptibility differences near tissue interfaces in the region of the midbrain cause a peak broadening and result in low-quality spectra compared with other brain regions in general. Additionally, the small dimension of the SN requires high-resolution MRS exactly co-registered with anatomical images. The few published studies about MRS in the region of the SN in PD patients used single-voxel spectroscopy (SVS) at 1.5 and 4 T respectively with volumes between 2.2 and 6 ml [18–20] and magnetic resonance spectroscopic imaging (MRSI) at 3 T with a nominal voxel size of 2.7 ml and 0.675 ml after matrix interpolation [21].

Goal of this study was to develop a method that can be used to investigate possible metabolic changes in the region of the SN in PD patients. Therefore, specially designed 3D-MRSI measurements were performed with a higher spatial resolution at 3 T to allow non-invasive detection and measurement of SN degeneration. Special care was taken to account for the known inhomogeneity issues, to minimise quality loss due to peak broadening.

Materials and methods

Subjects

Seventeen subjects (12 men, 5 women) aged between 51 and 79 years were included in the study. All subjects were classified into one of two groups: nine PD patients (mean 69±6.5 years, six men, three women) with disease durations between 4 and 25 years and Hoehn and Yahr stages 2.5 to 3, and eight age- and gender-matched neurologically healthy controls (mean 66± 10.8 years, six men, two women). The age difference between the two groups was not significant (p=0.459). Patients were underwent imaging in the medical ON state (while taking their medication as usual) to reduce tremor-related movement artefacts, after giving written informed consent in accordance with the local ethics committee. Initial high-resolution MRI of all subjects were obtained and examined by a neuroradiologist to exclude brain morphological abnormalities.

Data acquisition

All MR examinations were carried out at 3 T (Magnetom Tim Trio, Siemens Healthcare, Erlangen, Germany) with a 32-channel or a 12-channel receive-only phased array head coil in combination with the body coil for radio frequency transmission. The 12-channel head coil had to be used in some subjects because of the relatively small size of the 32-channel head coil. As only ratios were evaluated coil-dependent signal differences did not influence the results and the measurements were comparable.

Coronal (parallel to the midbrain axis), sagittal and transversal (perpendicular to the midbrain axis) T_2-weighted images were acquired using 2D high-resolution turbo spin echo (TSE) pulse sequences (TE=98 ms, TR= 4 s, field of view (FOV) $= 230 \times 230\,\mathrm{mm}^2$, matrix size $= 256 \times 256$, 19 slices, thickness=2 mm) for MRSI slice selection.

The proton 3D-MRSI was performed using a point resolved spectroscopy (PRESS) pulse sequence [22] with WET water saturation [23] and a short echo time TE=30 ms to reduce signal intensity loss by T_2 relaxation. For clinical application it is important to reduce the measurement time to an acceptable level for PD patients. Therefore, the repetition time (TR) chosen was relatively short (1350 ms). With this TR, the acquisition time (TA) could be reduced to 21:20 min. The short TR induces a T_1 weighting that usually has to be corrected for absolute quantification of metabolite concentrations. In this study only intra-individual ratios of peak integrals were evaluated.

The volume of interest (VOI) $= 40 \times 30 \times 30\ \mathrm{mm}^3$ was relatively small and could be fitted to the size of the midbrain. The exact planning procedure is shown in Fig. 1. The accurate localisation of the VOI was realised in each

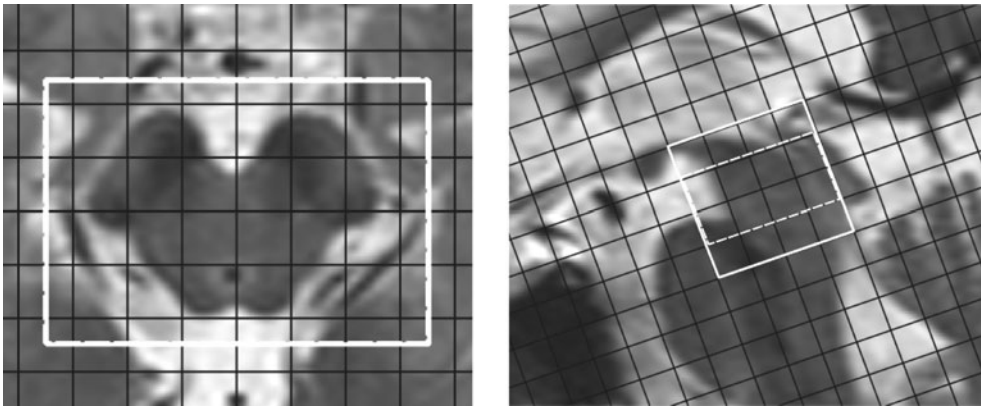

Fig. 1 MRSI planning schematic: Axial and sagittal T2-weighted MRI of the midbrain with PRESS box (*black grid*), volume of interest (*white box*), and adjustment volume (*dashed white box*) for the MRSI examination

subject so that the regions of the SN were located in the same voxels. The slice direction was parallel to the rostrocaudal SN dimension so that the voxel coordinates were exactly the same for each subject. Therefore, the inaccuracies in flip angles due to pulse profiles should be comparable and a correction would only be necessary for absolute quantification of metabolite concentrations.

To increase the effective spatial resolution and reduce partial volume effects the field of view $(\mathrm{FOV}) = 96 \times 96 \times 56\ \mathrm{mm}^3$ and the matrix size $= 16 \times 16 \times 8$ were chosen to be relatively large compared with the small VOI for a smaller point spread function (PSF) [24]. The nominal voxel size without interpolation was $6 \times 6 \times 7\ \mathrm{mm}^3$ and the number of averages NA=4.

In order to keep the acquisition time to an acceptable extent for clinical application, it was necessary to use elliptical weighted *k*-space sampling. Consequently, the high *k*-space frequencies were not acquired and the low *k*-space frequencies according to the apodisation during acquisition were more pronounced to favour sensitivity over detail and resolution. This reduction of acquired *k*-space data to 30% results in a larger effective voxel size than the nominal size. No Hamming filter was used.

Additionally, the carrier frequency was centred 2.0 ppm upfield from the water resonance (delta frequency=−2.0 ppm) between the Cr and NAA resonances to reduce chemical shift displacement artefacts. The acquisition bandwidth was 1000 Hz and acquisition duration was 1024 ms.

For the WET water saturation [23] a bandwidth=35 Hz was used without adjustment for water suppression resulting in a smaller excitation flip angle for water saturation. The residual water signals were high enough for all channels to determine the phase and combine all signal contributions of the multi-coil elements correctly so that no zero-order phase corrections were necessary.

In order to achieve appropriate magnetic field homogeneity, the volume for automatic and manual shimming procedures was adjusted to two slices of interest ($40 \times 30 \times 14\ \mathrm{mm}^3$). After shimming, the full width at half maximum (FWHM) of the water signal in the adjusted volume was smaller than 27 Hz in all cases. Neither fat saturation nor outer volume suppression was performed. The total measurement time of combined MRI/MRSI was approximately 30 min.

Spectra analysis

For post-processing and evaluation the Syngo software package on the MR scanner [25] was used. A fixed post-processing protocol was developed to avoid differences in data post-processing and curve fitting. Apodisation (time-domain filtering) with a Hanning filter of 200 ms width and zero-filling to 2048 data points were used to optimise the signal/noise ratio and the spectral resolution. The residual water signal was removed in the time domain by water subtraction. After Fourier transformation, an automatic baseline correction by a 6th order polynomial was performed. For integrating the NAA, Cr, Cho, and Ins resonances the spectra were fitted.

Based on the exact planning schema (Fig. 1) two enclosed voxels in the slice direction defined the rostral (upper part) and caudal (lower part) regions of the left and right SN. Consequently four voxels were analysed for each subject (Fig. 2).

The individual metabolite/Cr (NAA/Cr, Cho/Cr, Ins/Cr) ratios were determined for each voxel. Additionally, for intra-individual results the rostral-to-caudal ratios of the metabolite/Cr ratios were calculated. Furthermore, to evaluate potential metabolite changes between both slices the rostral-to-caudal ratios for each single metabolite (NAA, Cr, Cho, Ins) were determined. All values are given as mean ± standard deviation (SD).

To investigate the regional specificity the voxels in the rostral and the caudal parts of the midbrain tegmentum areas were also analysed.

Statistics

As a normal distribution of metabolite concentrations was assumed in both groups the mean values with standard deviations were calculated. Taking in consideration the

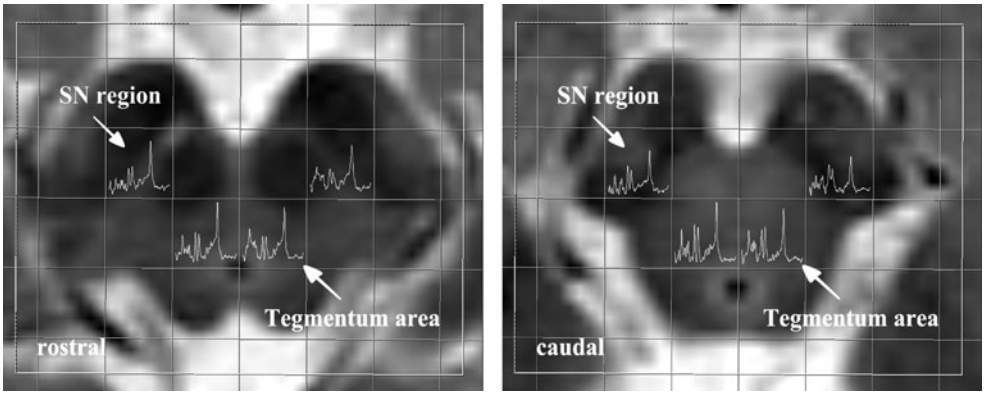

Fig. 2 Rostral (*left*) and caudal (*right*) voxels investigated in the regions of the substantia nigra as well as in the midbrain tegmentum areas

relatively small sample sizes, for statistical analysis an independent Wilcoxon-Mann–Whitney *u*-test with a statistical significance level of 0.05 was performed for significance testing.

Results

Proton 3D-MRSI spectra with acceptable quality and a nominal voxel size of 0.252 ml could be obtained in the rostral and caudal parts of the SN regions as well as the midbrain tegmentum areas in all subjects. The quality of the spectra was evaluated based on the FWHM of the NAA signal and was similar in healthy controls and PD patients, both in the SN regions and tegmentum areas: 16±2.4 Hz in controls, 17±2.3 Hz in PD patients (SN regions). Differences in line broadening could not be observed between the groups. Typical examples of ^{1}H-MRSI spectra in the SN regions of a healthy control and a PD patient are shown in Fig. 3. In a first visual inspection clear differences between the intra-individual NAA and Cr levels on the rostral and caudal SN parts could be recognised in both groups.

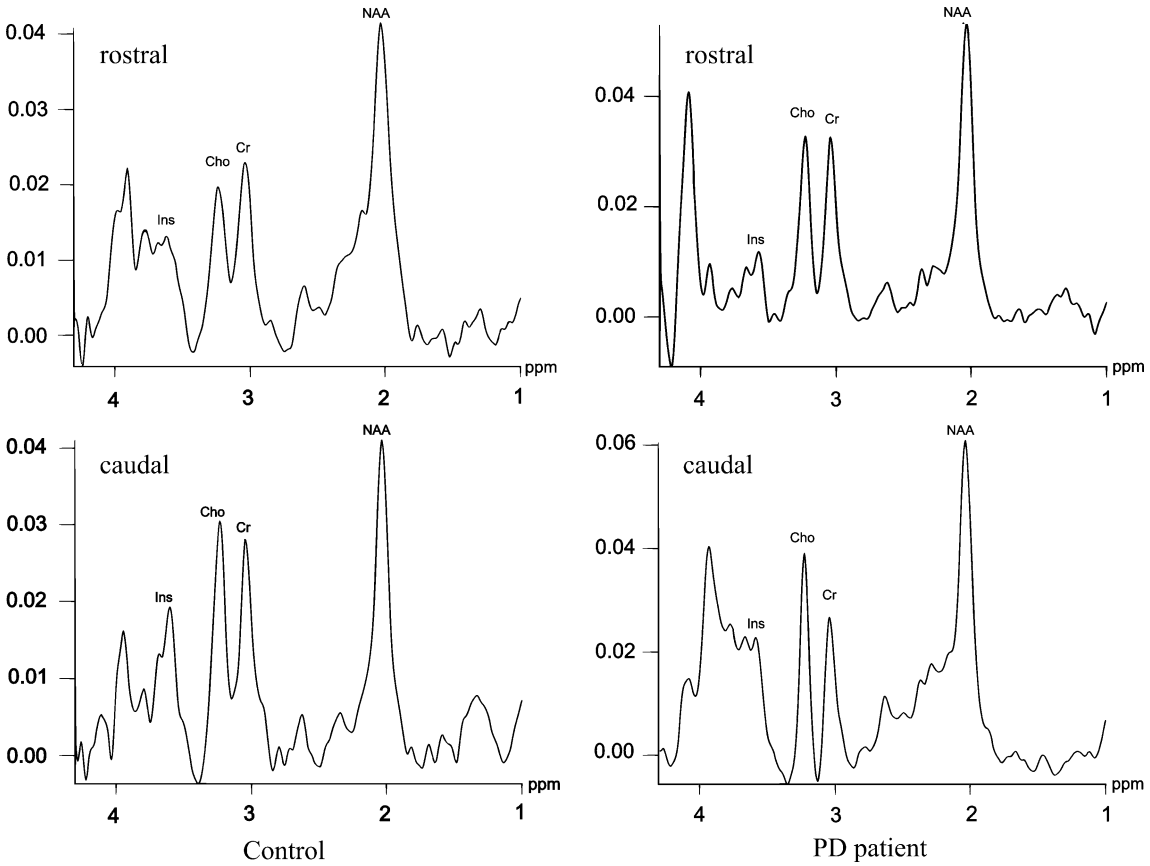

Fig. 3 ^{1}H-MRSI spectra in the rostral and caudal regions of the substantia nigra of a healthy control and a patient with Parkinson's disease acquired from 0.252 ml volumes. NAA = N-acetyl aspartate, Cr = creatine, Cho = choline, Ins = myo-inositol

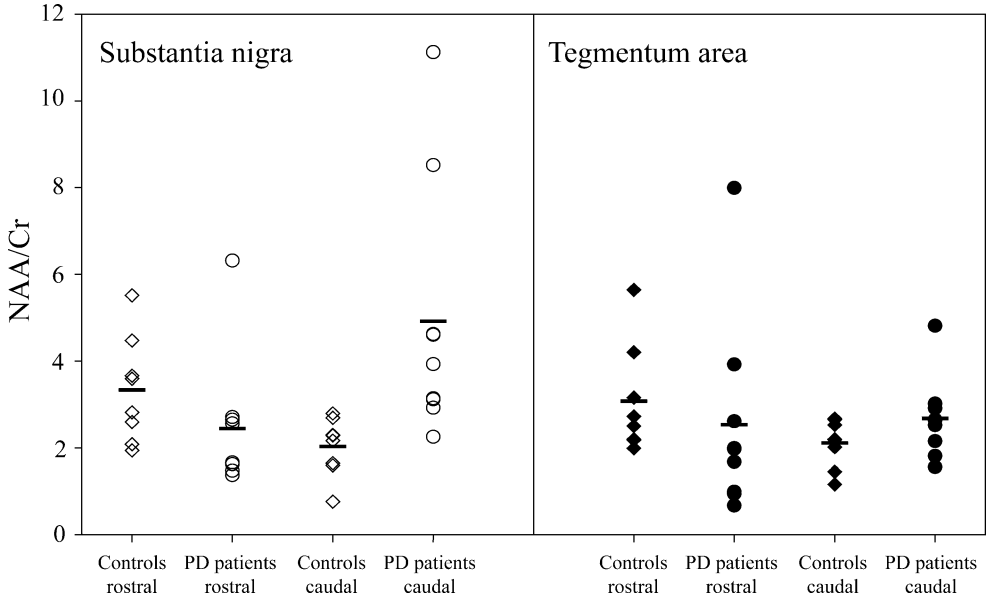

Fig. 4 Distribution of rostral and caudal NAA/Cr ratios with mean values in healthy controls (*rhombus*) and patients with Parkinson's disease (*circle*) in the regions of the substantia nigra and the midbrain tegmentum areas

The influence of surrounding tissue on signal intensity in a selected voxel was estimated by simulation. The measurement of a volume with 16×16×8 matrix points was assumed. The simulated object consisted of a box with the dimensions of a nominal voxel size and a signal intensity of 1 at the central position. All other positions within the object had an assumed intensity of 0. The *k*-space signal intensity of the object was calculated at all *k*-space positions. After 3D Fourier transformation, the neighbouring voxels (originally zero) showed signal intensities up to 12%. This value is the maximal contribution of each of the six neighbouring voxels to the signal intensity within the nominal voxel in the performed measurements.

The contributions from different coil elements were saved uncombined in a couple of cases to verify the automatic combination procedure. The residual water signal of each coil element was high enough to determine the exact phase, providing a correct signal combination in the resulting spectrum.

NAA/Cr ratios

Figure 4 shows that the NAA/Cr ratios overlap between both groups in the regions of the SN and in the tegmentum areas. The NAA/Cr ratios showed no significant differences between the two hemispheres, therefore only the averaged values for the SN regions are presented in Table 1. In the rostral SN regions, the PD patients showed a trend (p=0.054) towards decreased NAA/Cr ratios compared with healthy controls whereas in the caudal SN regions the NAA/Cr ratios were significantly increased (p=0.002) in PD patients compared with controls.

For quantification of these differences the intra-individual rostral-to-caudal ratios ($(NAA/Cr)_{rostral}/(NAA/Cr)_{caudal}$) were calculated (Table 1) and significant differences between the two groups could be found in the SN regions but not in the midbrain tegmentum areas (Fig. 5).

Cho/Cr and Ins/Cr ratios

The Cho/Cr and Ins/Cr ratios as well as the rostral-to-caudal ratios ($(Cho/Cr)_{rostral}/(Cho/Cr)_{caudal}$, $(Ins/Cr)_{rostral}/(Ins/Cr)_{caudal}$) are also given in Table 1. For the Ins/Cr ratios significant effects could be found as described earlier for NAA/Cr but with higher variations, most likely due to the limited accuracy of Ins estimations. Contrary to the

Table 1 Mean values with standard deviations of the rostral and caudal ratios of the metabolite/creatine ratios as well as the rostral-to-caudal ratios in the region of the substantia nigra in healthy controls and patients with Parkinson's disease, and the p values

	Controls	PD patients	P value
$(NAA/Cr)_{ros}$	3.34±1.23	2.45±1.55	0.054
$(NAA/Cr)_{cau}$	2.03±0.67	4.92±2.96	0.002
$(NAA/Cr)_{ros}/(NAA/Cr)_{cau}$	1.78±0.69	0.63±0.25	0.001
$(Cho/Cr)_{ros}$	0.85±0.12	1.08±0.40	0.162
$(Cho/Cr)_{cau}$	1.01±0.19	1.34±0.44	0.112
$(Cho/Cr)_{ros}/(Cho/Cr)_{cau}$	0.93±0.24	0.86±0.18	0.962
$(Ins/Cr)_{ros}$	0.82±0.43	0.59±0.52	0.248
$(Ins/Cr)_{cau}$	0.64±0.34	1.95±1.43	0.021
$(Ins/Cr)_{ros}/(Ins/Cr)_{cau}$	1.73±1.30	0.48±0.69	0.034

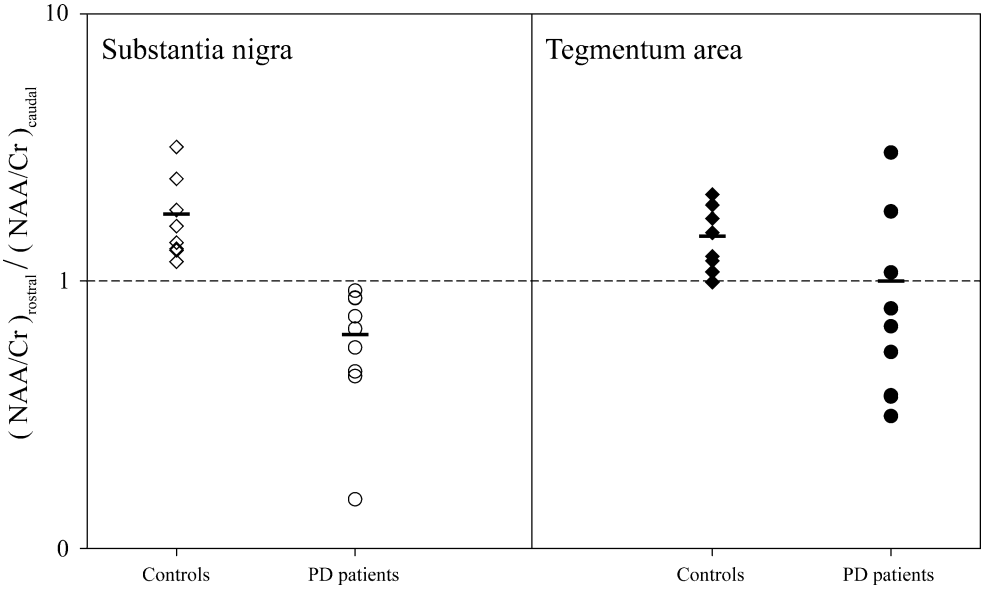

Fig. 5 Logarithmic plot of the rostral-to-caudal ratios of the NAA/Cr ratios with mean values in healthy controls (*rhombus*) and patients with Parkinson's disease (*circle*) in the regions of the substantia nigra and the midbrain tegmentum areas

NAA/Cr and Ins/Cr ratios, the Cho/Cr ratios showed no significant differences (p=0.962) between the two groups.

Single metabolite ratios

To investigate the causes of these group-specific differences the single metabolite ratios between the rostral and caudal regions ($metabolite_{rostral}/metabolite_{caudal}$) of the SN were calculated. These rostral-to-caudal ratios for all four metabolites are represented in Table 2. The ratios for NAA and Cr were significantly different (p=0.001 and p=0.001) for both groups, however with different directions. These contrary effects between NAA and Cr as well as between Ins and Cr seem to cause the clear separation.

Discussion

This study demonstrated the feasibility of obtaining short-echo ^{1}H-MRSI spectra of acceptable quality in the regions of SN and midbrain tegmentum areas of healthy controls and PD patients with a nominal voxel size of 0.252 ml at 3 T. The analysis of spectra from the rostral and caudal parts of the SN showed significant differences between the two groups.

Artefacts and shimming difficulties caused by local magnetic field inhomogeneities could be reduced by using a voxel size that was relatively small compared with the spatial field distortions. Some technical limitations of the spatial resolution could be avoided by using 3D-MRSI instead of SVS. Susceptibility effects due to higher iron concentrations in the SN led to an expected marginal line broadening compared with known FWHM values. However, the line widths of the NAA signals in all spectra as well as the line widths of the water signal during the manual shimming procedure were comparable in both groups [26, 27].

The effective voxel size was larger than the nominal size because of the reduced k-space sampling, which was needed to reduce the measurement time to an acceptable in vivo level. Therefore, the relatively high overlap in effective voxel volumes yields to a weighted averaging of metabolite signals from adjusted positions. This overlap is larger in slice direction because of the small number of slices. As an effect of this signal overlap, existing differences in neighboured voxels were diminished. Nevertheless, there were still significant differences between PD patients and healthy controls. The investigated voxels in the rostral slice were influenced by partial volume effects from the caudal slice and from the slice inside the cerebrospinal fluid (CSF). The partial volume effect by CSF reduces the absolute metabolite levels but no changes in the metabolite/Cr ratios have to be expected. The investigated voxels in the caudal slice were influenced by

Table 2 Rostral-to-caudal ratios (mean values with standard deviations) of the metabolites in the region of the substantia nigra in healthy controls and patients with Parkinson's disease, and the p values

	NAA_{ros}/NAA_{cau}	Cr_{ros}/Cr_{cau}	Cho_{ros}/Cho_{cau}	Ins_{ros}/Ins_{cau}
Controls	1.38±0.16	0.88±0.21	0.83±0.32	1.46±1.25
PD patients	0.89±0.19	1.98±1.10	1.60±0.99	0.77±1.25
P value	0.001	0.001	0.011	0.054

partial volume effects from the rostral slice and from the caudal slice inside the pons. The partial volume effects from the pons could change the metabolite/Cr ratios. However, this inaccuracy should be the same in healthy controls and PD patients as neuropathological processes in PD are described for the SN but not for the pons. A further reduction of the effective voxel size should provide a much better separation at the cost of longer measurement times.

For clinical application of the described MRSI method it was necessary to reduce the acquisition time to an acceptable time period for PD patients. Various possibilities exist to reduce the total measurement time. For instance a small matrix size can be chosen, which yields a broad PSF and consequently a large effective voxel size at the cost of high partial volume effects. Another possibility would be to reduce the repetition time TR, which leads to a reduced signal/noise ratio because of the long T_1 relaxation times of the metabolites [28]. In this study TR was 1350 ms and caused a reduction of the NAA signal intensity of 37%. A further reduction of TR to 800 ms would decrease the NAA signal intensity by 55%. One more option is to reduce *k*-space sampling, which leads to the disadvantages discussed. However, to maximise spatial resolution and minimise acquisition time a combination of all methods yields the best results.

As absolute metabolite quantification was not needed in this study, metabolite levels were not corrected for T_1 weighting. However, alterations of T_1 relaxation times in the SN could be one reason for the differences found between PD patients and healthy controls and should be investigated in future studies.

Problems in the quantification of MRSI data acquired at short echo time and moderate magnetic field strength appear by complex multiplet resonance patterns, overlapping metabolites, variations in the line shape and underlying baseline variations. The largest variability showed Ins and was not reliable enough to use for NAA/Ins ratios. Additionally, the broad spectral pattern cannot be measured accurately using only a single peak. Furthermore, the short T_2 relaxation time of Ins [28] leads at TE=30 ms to an intensity loss of 24%. For comparison the loss in signal intensity of NAA is only 13%, assuming a T_2 of 221 ms [28]. However, the echo time TE was already at the minimum at the chosen set-up and a further reduction was not possible.

T_2 relaxation times in the human brain depend on age, brain region [29] and pathological features. To account for age- and region-specific influences on T_2, an age-matched control group was chosen and the anatomical location measured was chosen with great care. Segmentation and subsequent correction for tissue composition was not necessary because of exact voxel localisation inside the SN region.

Previous MRS studies in the midbrain encountered problems obtaining spectra with acceptable quality because of the unfavourable small and heterogeneous region as well as the high cellular iron content of the SN [16]. The magnetic field homogeneity is poor [17] and spectra with high line widths and signal overlaps were obtained. Oz et al. [18] used SVS and found trends towards decreased NAA and increased Cho levels in PD patients compared with healthy controls. Hattingen et al. [21] found trends towards reduced phosphocreatine levels in ^{31}P MRSI as well as decreased total Cr levels in ^{1}H MRSI in the midbrain of PD patients with advanced disease duration. O'Neill et al. [19] observed significantly decreased Cr levels in PD patients compared with normal controls using SVS and followed from this that elevated NAA/Cr ratios in the SN region of PD patients reported earlier by Choe et al. [20] were rather due to lower Cr than to higher NAA concentrations. The results of the present study cannot be compared directly with previous data [18–21]. In previous studies the voxel size used was larger and distinct parts of the SN could not be examined and compared with each other.

Nevertheless, all measuring inaccuracies were identical in both groups but there were still significant differences between PD patients and healthy controls. So far, neither absolute quantification, whether the differences were really in NAA and Cr or only in metabolites or macromolecules underlying these main metabolites, nor biochemical explanation for the results can be given. These questions should form the basis for further investigations with larger cohorts to increase statistical power.

In addition to the established imaging methods like positron emission tomography, single-photon emission tomography, and transcranial sonography which support the diagnosis of Parkinson's disease the application of the presented MRSI method could contribubute to the enhancement of the diagnostic accuracy and monitoring the disease progression.

In conclusion, the present study offers a method that allows the acquisition of MR spectra with a high spatial resolution in a three-dimensional grid of the midbrain. Evaluation of ratios of metabolite signals from different rostral and caudal regions reliably differentiate between PD patients and healthy controls in a first small sample.

References

1. Hughes AJ, Daniel SE, Kilford L, Lees AJ (1992) Accuracy of clinical diagnosis of idiopathic Parkinson's disease: a clinico-pathological study of 100 cases. J Neurol Neurosurg Psychiatry 55:181–184
2. O'Keeffe GC, Michell AW, Barker RA (2009) Biomarkers in Huntington's and Parkinson's Disease. Ann NY Acad Sci 1180:97–110

3. Jankovic J, Rajput AH, McDermott MP, Perl DP (2000) The evolution of diagnosis in early Parkinson disease. Parkinson Study Group. Arch Neurol 57:369–372
4. Meara J, Bhowmick BK, Hobson P (1999) Accuracy of diagnosis in patients with presumed Parkinson's disease. Age Ageing 28:99–102
5. Auer DP (2009) In vivo imaging markers of neurodegeneration of the substantia nigra. Exp Gerontol 44:4–9
6. Jansen JF, Kooi ME, Kessels AG, Nicolay K, Backes WH (2007) Reproducibility of quantitative cerebral T2 relaxometry, diffusion tensor imaging, and 1H magnetic resonance spectroscopy at 3.0 Tesla. Invest Radiol 42:327–337
7. Moffett JR, Ross B, Arun P, Madhavarao CN, Namboodiri AM (2007) N-Acetylaspartate in the CNS: from neurodiagnostics to neurobiology. Prog Neurobiol 81:89–131
8. Charles HC, Lazeyras F, Krishnan KR, Boyko OB, Patterson LJ, Doraiswamy PM, McDonald WM (1994) Proton spectroscopy of human brain: effects of age and sex. Prog Neuropsychopharmacol Biol Psychiatry 18:995–1004
9. Leary SM, Brex PA, MacManus DG, Parker GJ, Barker GJ, Miller DH, Thompson AJ (2000) A (1)H magnetic resonance spectroscopy study of aging in parietal white matter: implications for trials in multiple sclerosis. Magn Reson Imaging 18:455–459
10. Ferguson KJ, MacLullich AM, Marshall I, Deary IJ, Starr JM, Seckl JR, Wardlaw JM (2002) Magnetic resonance spectroscopy and cognitive function in healthy elderly men. Brain 125:2743–2749
11. Lazeyras F, Charles HC, Tupler LA, Erickson R, Boyko OB, Krishnan KR (1998) Metabolic brain mapping in Alzheimer's disease using proton magnetic resonance spectroscopy. Psychiatry Res 82:95–106
12. Brand A, Richter-Landsberg C, Leibfritz D (1993) Multinuclear NMR studies on the energy metabolism of glial and neuronal cells. Dev Neurosci 15:289–298
13. Broom KA, Anthony DC, Lowe JP, Griffin JL, Scott H, Blamire AM, Styles P, Perry VH, Sibson NR (2007) MRI and MRS alterations in the preclinical phase of murine prion disease: association with neuropathological and behavioural changes. Neurobiol Dis 26:707–717
14. Mao H, Toufexis D, Wang X, Lacreuse A, Wu S (2007) Changes of metabolite profile in kainic acid induced hippocampal injury in rats measured by HRMAS NMR. Exp Brain Res 183:477–485
15. Massey LA, Yousry TA (2010) Anatomy of the substantia nigra and subthalamic nucleus on MR imaging. Neuroimaging Clin N Am 20:7–27
16. Hallgren B, Sourander P (1958) The effect of age on the non-haemin iron in the human brain. J Neurochem 3:41–51
17. Ordidge RJ, Gorell JM, Deniau JC, Knight RA, Helpern JA (1994) Assessment of relative brain iron concentrations using T2-weighted and T2*-weighted MRI at 3 Tesla. Magn Reson Med 32:335–341
18. Oz G, Terpstra M, Tkác I, Aia P, Lowary J, Tuite PJ, Gruetter R (2006) Proton MRS of the unilateral substantia nigra in the human brain at 4 tesla: detection of high GABA concentrations. Magn Reson Med 55:296–301
19. O'Neill J, Schuff N, Marks WJ Jr, Feiwell R, Aminoff MJ, Weiner MW (2002) Quantitative 1H magnetic resonance spectroscopy and MRI of Parkinson's disease. Mov Disord 17:917–927
20. Choe BY, Park JW, Lee KS, Son BC, Kim MC, Kim BS, Suh TS, Lee HK, Shinn KS (1998) Neuronal laterality in Parkinson's disease with unilateral symptom by in vivo 1H magnetic resonance spectroscopy. Invest Radiol 33:450–455
21. Hattingen E, Magerkurth J, Pilatus U, Mozer A, Seifried C, Steinmetz H, Zanella F, Hilker R (2009) Phosphorus and proton magnetic resonance spectroscopy demonstrates mitochondrial dysfunction in early and advanced Parkinson's disease. Brain 132:3285–3297
22. Duijn JH, Matson GB, Maudsley AA, Weiner MW (1992) 3D phase encoding 1H spectroscopic imaging of human brain. Magn Reson Imaging 10:315–319
23. Ogg RJ, Kingsley PB, Taylor JS (1994) WET, a T1- and B1-insensitive water-suppression method for in vivo localized 1H NMR spectroscopy. J Magn Reson B 104:1–10
24. Mareci TH, Brooker HR (1991) Essential considerations for spectral localization using indirect gradient encoding of spatial information. J Magn Reson 92:229–246
25. Fayed N, Modrego PJ, Medrano J (2009) Comparative test-retest reliability of metabolite values assessed with magnetic resonance spectroscopy of the brain. The LCModel versus the manufacturer software. Neurol Res 31:472–477
26. Galazka-Friedman J, Friedman A, Bauminger ER (2009) Iron in the brain. Hyperfine Interact 189:31–37
27. Friedman A, Galazka-Friedman J, Koziorowski D (2009) Iron as a cause of Parkinson disease—a myth or a well established hypothesis? Parkinsonism Relat Suppl Disord 15:S212–S214
28. Träber F, Block W, Lamerichs R, Gieseke J, Schild HH (2004) 1H metabolite relaxation times at 3.0 tesla: measurements of T1 and T2 values in normal brain and determination of regional differences in transverse relaxation. J Magn Reson Imaging 19:537–545
29. Kirov II, Fleysher L, Fleysher R, Patil V, Liu S, Gonen O (2008) Age dependence of regional proton metabolites T2 relaxation times in the human brain at 3 T. Magn Reson Med 60:790–795